Journal of Electronic Materials (2022) 51:2716–2731
https://doi.org/10.1007/s11664-022-09534-6

TOPICAL COLLECTION: SYNTHESIS AND ADVANCED CHARACTERIZATION OF MAGNETIC OXIDES

Synthesis and Characterization of $(1-x)Bi_{1/2}Na_{1/2}TiO_3+xSrNiO_{3-\delta}$ Solid Solution System

Dang Duc Dung[1] · Nguyen Hoang Thoan[1] · Nguyen Quoc Dung[2] · Nguyen Huu Lam[1] · Vu Tien Lam[1] · Pham Van Vinh[3] · Pham Dinh Luong[1] · Duong Quoc Van[4]

Received: 5 November 2021 / Accepted: 17 February 2022 / Published online: 22 March 2022

Abstract

In this report, solid solutions of $(1-x)Bi_{1/2}Na_{1/2}TiO_3+xSrNiO_{3-\delta}$ materials were synthesized by a chemical method. X-ray diffraction and Raman scattering were used to study the structural properties of the $(1-x)Bi_{1/2}Na_{1/2}TiO_3+xSrNiO_{3-\delta}$ solid solutions. All studied samples had rhombohedral symmetry, where the Sr and Ni cations tended to randomly incorporate with the host $Bi_{1/2}Na_{1/2}TiO_3$ lattices during the formation of solid solutions. The random incorporation of Sr and Ni cations into the host lattices resulted in structural distortion and reduced the optical band gap from 3.04 eV for the pure $Bi_{1/2}Na_{1/2}TiO_3$ to 2.63 eV for the 9 mol.% $SrNiO_{3-\delta}$-modified $Bi_{1/2}Na_{1/2}TiO_3$ sample. The complex magnetic properties of $(1-x)Bi_{1/2}Na_{1/2}TiO_3+xSrNiO_{3-\delta}$ system were investigated as a function of $SrNiO_{3-\delta}$ concentrations. We expected that our simple and flexible method could be used to integrate the ferromagnetic properties in current advanced functional lead-free materials.

Keywords $Bi_{1/2}Na_{1/2}TiO_3$ · $SrNiO_{3-\delta}$ · ferromagnetism · lead-free ferroelectric · sol-gel

Introduction

Lead-free ferroelectric $Bi_{1/2}Na_{1/2}TiO_3$-based materials are environmentally friendly and less harmful to the human body than $Pb(Zr,Ti)O_3$-based materials.[1,2] Because they have good piezoelectric (piezoelectric coefficient d_{33} of 74.0–94.8 pC/N), ferroelectric (large remnant polarization P_r of 38 μC/cm^2 and a high Curie temperature T_C of 320°C), and dielectric properties (dielectric constants ε at room temperature of 425), the $Bi_{1/2}Na_{1/2}TiO_3$-based materials are currently active in replacing $Pb(Zr,Ti)O_3$-based materials in electronics devices.[1,3] Recently, $Bi_{1/2}Na_{1/2}TiO_3$ materials showed promise in extending functional materials due to observation of room-temperature ferromagnetism.[3] The observation of room-temperature ferromagnetism in lead-free $Bi_{1/2}Na_{1/2}TiO_3$ ferroelectric materials is very important for transferring materials to the next general electronic devices, where the magnetization is controlled by an applied external electric field, and vice versa, the electrical polarization is tuned by an applied external magnetic fields such as magnetic field sensors, mechanical ME antennas, or nonvolatile memory.[4] However, the current issue of using lead-free ferroelectric $Bi_{1/2}Na_{1/2}TiO_3$ materials by converting magnetoelectric behaviors is that the magnetization of about 1 memu/g at room temperature is too small and has a strong influence on diamagnetic components.[3,5] Thus, improving magnetization of lead-free ferroelectric $Bi_{1/2}Na_{1/2}TiO_3$-based materials is an important requirement for the development of their magnetic performance. There are two simple ways to improve the magnetic moment of

✉ Dang Duc Dung
dung.dangduc@hust.edu.vn

✉ Duong Quoc Van
vandq@hnue.edu.vn

1 Multifunctional Ferroics Materials Lab., School of Engineering Physics, Hanoi University of Science and Technology, 1 Dai Co Viet Road, Hanoi, Vietnam

2 Department of Chemistry, Thai Nguyen University of Education, Thai Nguyen City, Vietnam

3 Faculty of Engineering Physics and Nanotechnology, VNU University of Engineering and Technology, 144 Xuan Thuy road, Cau Giay district, Hanoi, Vietnam

4 Faculty of Physics, Hanoi National University of Education, 136 Xuan Thuy Road, Hanoi, Vietnam

lead-free ferroelectric $Bi_{1/2}Na_{1/2}TiO_3$ materials, including compositing and doping methods.[6]

By compositing, ferromagnetic phases are distributed in a matrix of lead-free ferroelectric phases, thus improving the magnetic moment of lead-free ferroelectric $Bi_{1/2}Na_{1/2}TiO_3$ materials such as $Bi_{1/2}Na_{1/2}TiO_3$-$CoFe_2O_4$ or $Bi_{1/2}Na_{1/2}TiO_3$-$NiFe_2O_4$ systems.[7,8] In addition, the performance of lead-free ferroelectric $Bi_{1/2}Na_{1/2}TiO_3$ materials is improved by compositing such as expansion to $0.97(Bi_{1/2}Na_{1/2}TiO_3)$-$0.03(K_{0.47}Na_{0.47}Li_{0.06}Nb_{0.74}Sb_{0.06}Ta_{0.2}O_3)$ or $[72.5(Bi_{1/2}Na_{1/2}TiO_3)$-$22.5(Bi_{1/2}K_{1/2}TiO_3)$-$5(BiMg_{1/2}Ti_{1/2}O_3)]$ and instead of ferrite spinel $CoFe_2O_4$ by modified-ferrite spinel $Co_{0.6}Zn_{0.4}Fe_{1.7}Mn_{0.3}O_4$.[9,10] However, the main problem is that high leakage current in the composites due to interface defects between ferroelectric/ferromagnetic grains leads to a low polarized electric field because of the hindrance of dipole alignments.[7–11] Therefore, the magnetic properties of lead-free ferroelectric $Bi_{1/2}Na_{1/2}TiO_3$ materials should be improved by doping methods.[5,12–17]

The magnetic moment of lead-free ferroelectric $Bi_{1/2}Na_{1/2}TiO_3$ materials has recently been significantly improved by incorporating transition metals into Ti-sites.[5,12–17] However, the origin of the ferromagnetic order by interactions with transition metal cations is still unclear, even though the magnetization of lead-free ferroelectric $Bi_{1/2}Na_{1/2}TiO_3$ materials increases, where various possible sources are favored for the magnetic order. Wang et al. reported that observation in ferromagnetic ordering at room temperature via Fe-doped lead-free ferroelectric $Bi_{1/2}Na_{1/2}TiO_3$ materials as possible from the interaction of Fe^{3+} cations through oxygen vacancies.[12] In contrast, in another study by Wang et al., they also pointed out that the ferromagnetic ordering at room temperature in the case of Co-doped lead-free ferroelectric $Bi_{1/2}Na_{1/2}TiO_3$ materials originated from ferromagnetic Co clusters.[13] Dung et al. reported that ferromagnetic behaviors were obtained at room temperature for Fe-, Co- and Ni-doped $Bi_{1/2}Na_{1/2}TiO_3$ materials, where the complex interaction of transition ions through oxygen vacancies (□) was favored for the ferromagnetic order, while the magnetic polarons were super-interactions to favor an antiferromagnetic-like behavior.[14–16] Thanh et al. also pointed out that the magnetic properties of lead-free ferroelectric $Bi_{1/2}Na_{1/2}TiO_3$ materials possibly resulted from the interactions of $Mn^{2+/3+}$ cations through oxygen vacancies, e.g., Mn^{2+}-□-Mn^{2+} or Mn^{2+}-□-Mn^{3+}.[17] In addition, Thanh et al. suggested that oxygen vacancies could induce non-zero magnetic moments when studying the influence of Cr impurity on the magnetic properties of $Bi_{1/2}Na_{1/2}TiO_3$ materials.[5] However, the number of transition metals in the periodic table poses a limitation in the magnetic sources for injection of the magnetic properties of lead-free ferroelectric $Bi_{1/2}Na_{1/2}TiO_3$ materials. Moreover, so far, the role of *A*-site and *B*-site co-controlling via alkaline-earth and transition metals, respectively, on the magnetic properties of lead-free ferroelectric $Bi_{1/2}Na_{1/2}TiO_3$ materials are not well reported.

Thanks to the solid solution with various ABO_3-type materials, the magnetic moment of $Bi_{1/2}Na_{1/2}TiO_3$ materials recently has been greatly enhanced. Hue et al. reported that the magnetic properties of $Bi_{1/2}Na_{1/2}TiO_3$ materials were increased by solid solution with ilmenite-type $MTiO_3$ (M=Ni and Mn).[18,19] The results were also consistent with ilmenite-type $FeTiO_3$-modified $Bi_{1/2}Na_{1/2}TiO_3$ materials.[20] Based on their reports, the ferromagnetic properties of $Bi_{1/2}Na_{1/2}TiO_3$ materials are enhanced from the interaction of transition metal cations through oxygen vacancies (□), e.g., Fe^{3+}-□-Fe^{3+}, Ni^{2+}-□-Ni^{2+}, or Mn^{3+}-□-Mn^{3+} or super interaction between Fe^{3+}-□-Fe^{3+} versus Fe^{3+}-□-Fe^{3+} e.g., like-magnetic polaron interaction but also from *A*-site vacancies.[18–20] In addition, observation of an anti-ferromagnetic-like transition metal for high doping concentration is possibly related to the magnetic polaron of super interaction between ferromagnetic pairs, e.g. Fe^{3+}-□-Fe^{3+} versus Fe^{3+}-□-Fe^{3+}.[18–20] The complex *A*-site vacancy (Bi, Na) disorder results in strong enhancement of the magnetic moments compared with only a single transition metal incorporated with Ti-sites.[14–20] In addition, the magnetic properties of $Bi_{1/2}Na_{1/2}TiO_3$ materials have been reported to be strongly influenced via co-modification by alkaline earth and transition metals at both (Bi, Na)-sites and Ti-sites.[21–28] The role of substitution of alkaline earth cations into the host lattice of $Bi_{1/2}Na_{1/2}TiO_3$ materials is complicated due to the compensation of charges and ionic radii. The substitution of alkaline earth, including Mg^{2+}, Sr^{2+}, Ca^{2+}, and Ba^{2+} cations, for Bi^{3+}-sites, creates oxygen vacancies, while those incorporated with Na^{+}-sites generate Na vacancies.[21–28] Recently, both experimental and theoretical calculation studies well explained the archived ferromagnetism of Na vacancies.[3,21] The oxygen vacancies do not show ferromagnetism but favor reducing the valence state of Ti^{4+} to Ti^{3+}, resulting in large magnetic moments.[21,26]

Among alkaline-earth perovskite-type materials, alkaline-earth nickel-based perovskite-type $ANiO_{3-\delta}$ materials are interesting because of the complex magnetic properties that depend on the alkaline-earth cations and the valence states of Ni cations.[29] Among alkaline-earth nickel-based perovskite-type $ANiO_{3-\delta}$ materials, $SrNiO_{3-\delta}$ materials exhibit various structural and magnetic ground states as a function of oxygen deficiencies such as $SrNiO_2$, $SrNiO_{2.5}$ (or $Sr_2Ni_2O_5$), and $SrNiO_3$.[30–34] Rahman et al. reported that $SrNiO_2$ materials exhibited antiferromagnetic order with the Neel temperature (T_N) of 85 K.[30] However, Anisimov et al. reported that the ground state of $SrNiO_2$ was found to be a diamagnetic insulator.[34] Chen et al. predicted that the hexagonal $SrNiO_3$ exhibited half-metallic with ferromagnetic states.[33] So far, various alkaline-earth perovskite-type

materials (e.g. $AFeO_{3-\delta}$; $ACoO_{3-\delta}$ and $AMnO_{3-\delta}$) have been reported to enhance the magnetic moment of lead-free ferroelectric $Bi_{1/2}Na_{1/2}TiO_3$ materials. However, so far, there is still no report on the influence of $SrNiO_{3-\delta}$ on the magnetic properties of the host $Bi_{1/2}Na_{1/2}TiO_3$ materials. By incorporating solid solute alkaline-earth $SrNiO_{3-\delta}$ materials into host $Bi_{1/2}Na_{1/2}TiO_3$ materials, one expects to inject the ferromagnetism into $Bi_{1/2}Na_{1/2}TiO_3$ materials via co-modification of Sr cations at (Bi, Na)-sites and Ni cations at Ti-sites.

In this work, the binary $(1-x)$ $Bi_{1/2}Na_{1/2}TiO_3$ $+xSrNiO_{3-\delta}$ solid solutions were synthesized by sol-gel technique. The random incorporation of Sr and Ni cations into the $Bi_{1/2}Na_{1/2}TiO_3$ host lattices resulted in a reduction of optical band gap and complex influence of room-temperature ferromagnetism.

Experimental

The $(1-x)Bi_{1/2}Na_{1/2}TiO_3+xSrNiO_{3-\delta}$ solid solutions (namely, pure BNT, and BNT-$xSrNiO_{3-\delta}$; x=0.5%; 1%; 3%; 5%; 7% and 9 mol.%) were synthesized by sol-gel technique. The starting chemicals included bismuth(III) nitrate pentahydrate ($Bi(NO_3)_3.6H_2O$, Sigma-Aldrich, 98%), sodium nitrate ($NaNO_3$, Sigma-Aldrich, ≥ 99.0%), strontium nitrate ($Sr(NO_3)_2$, Sigma-Aldrich, ≥ 99.0%), nickel(II) nitrate hexahydrate ($Ni(NO_3)_2.6H_2O$, Sigma-Aldrich, ≥ 98.5%), and titanium(IV) isopropoxide ($C_{12}H_{28}O_4Ti$, Sigma-Aldrich, 97%). Acetic acid (CH_3COOH, Sigma-Aldrich, 99%) and acetylacetone ($CH_3COCH_2COCH_3$, Sigma-Aldrich, ≥ 99%) were selected as ligands for our experiments. At first, $Bi(NO_3)_3.6H_2O$ was weighed and dissolved in a mixing solution of acetic acid with deionized water (by volume ratio of 1:5) by magnetic stirring. Subsequently, $Sr(NO_3)_2$ and $NaNO_3$ were weighed and dissolved in the solution. Sodium is a light element that is easy to evaporate during gelling and sintering processes that make non-stoichiometric composition.[14–28] Thus, the sodium component was weighed to an amount around 40–50 mol.% larger than the initial-estimated $NaNO_3$ amount.[14–28] To prevent hydroxylation of Ti^{4+} cations, acetylacetone was added to the solution before dropping the desired $C_{12}H_{28}O_4Ti$ solution. The solution was magnetically stirred until becoming transparent before adding $Ni(NO_3)_2.6H_2O$. The final solutions were continuously magnetically stirred for around 3–4 h before drying in an oven at around 100°C to form dry gels. Powder samples were obtained by annealing the dry gels at 900°C for 3 h in the air. The chemical composition of powder samples was determined by energy dispersion x-ray spectroscopy (EDX) and further confirmed using an electron probe micro-analyzer (EPMA). The crystal structural symmetry of samples was studied by x-ray diffraction (XRD) and Raman scattering. The optical properties of the samples were investigated by both absorption spectroscopy (UV–Vis) and photoluminescence (PL). The magnetic properties of samples were measured by a vibrating sample magnetometer (VSM). All measurements were performed at room temperature.

Results and Discussion

The chemical composition of the pure $Bi_{1/2}Na_{1/2}TiO_3$ and $SrNiO_{3-\delta}$-modified $Bi_{1/2}Na_{1/2}TiO_3$ materials was determined by EDX measurements. Figure 1a and b showed EDX spectra of the pure $Bi_{1/2}Na_{1/2}TiO_3$ sample and the BNT-5%$SrNiO_{3-\delta}$ sample. The inset of each figure showed an area selected for chemical composition measurements. The EDX spectrum of the pure BNT sample exhibited typical peaks of constituent elements, including Bi, Na, Ti, and O. In addition, the EDX spectrum of BNT-5%$SrNiO_{3-\delta}$ exhibited two additional typical peaks for Sr and Ni, which was clear evidence for the presence of impurity cations in the host material.

The distribution of Sr and Ni impurity cations in the $Bi_{1/2}Na_{1/2}TiO_3$ host matrix is shown in Fig. 2 for chemical mapping of the BNT-5%$SrNiO_{3-\delta}$ sample. The chemical mappings of the host elements, Bi, Na, Ti, and O, and impurity elements Ni and Sr are shown in Fig. 2b–g, respectively, while the image of the selected area for chemical mappings is shown in Fig. 2a. The results indicate that the chemical elements of the host and addition components were homogeneously distributed. In other words, the chemical mapping

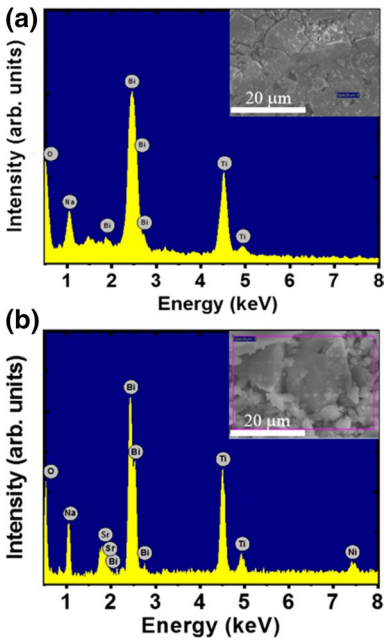

Fig. 1 Energy-dispersive x-ray spectra of (a) pure $Bi_{1/2}Na_{1/2}TiO_3$ and (b) 5 mol.%-$SrNiO_{3-\delta}$-modified $Bi_{1/2}Na_{1/2}TiO_3$ materials. The selected areas on samples for chemical determination are shown in the insets of each figure, respectively.

images provided solid evidence for the homogeneous distribution of additional elements into the host materials.

Furthermore, the random distribution of Sr and Ni cations in the host $Bi_{1/2}Na_{1/2}TiO_3$ lattices was investigated using XRD. XRD patterns of the pure $Bi_{1/2}Na_{1/2}TiO_3$ and $SrNiO_{3-\delta}$-modified $Bi_{1/2}Na_{1/2}TiO_3$ materials with various $SrNiO_{3-\delta}$ concentrations are shown in Fig. 3a. Based on the positions and relative intensity of diffraction peaks, the pure $Bi_{1/2}Na_{1/2}TiO_3$ material was determined to have rhombohedral symmetry. This result is consistent with recent reports for the $Bi_{1/2}Na_{1/2}TiO_3$ materials synthesized by the sol-gel technique.[14–28] No additional peak was observed after $SrNiO_{3-\delta}$ addition, indicating that the $SrNiO_{3-\delta}$-modified $Bi_{1/2}Na_{1/2}TiO_3$ materials had the same structure as the pure $Bi_{1/2}Na_{1/2}TiO_3$ material. The results also demonstrated that no secondary and/or impurity phase was detected under XRD resolution. In other words, $SrNiO_{3-\delta}$ was well incorporated in the host $Bi_{1/2}Na_{1/2}TiO_3$ materials. To further confirm the random incorporation of Sr and Ni cations into the host $Bi_{1/2}Na_{1/2}TiO_3$ lattices, the diffraction spectra were enlarged in the 2θ-range of 31.0°–34.0° as shown in Fig. 3b. The figure indicates that the satellite (012)/(110) peaks of the rhombohedral structure overlapped. Each diffraction peak was well distinguished by Lorentzian fitting with *r*-squared greater than 0.99, as shown by blue lines in Fig. 3b. The couple (012)/(110) peak position tended to shift to a lower diffraction 2θ-angle with increasing $SrNiO_{3-\delta}$ concentration, indicating an expansion of lattice parameters. The lattice parameter distortion of the $Bi_{1/2}Na_{1/2}TiO_3$ materials could be explained by considering the radius difference between Sr and Ni impurity cations and the host cations (Ba, Na, and Ti). Based on Shannon's report, Bi and Na cations located at *A*-sites have radii of 1.17 Å (in the coordination of VIII) and 1.39 Å (in the coordination of XII), respectively.[35] Ti cations located at *B*-sites (in the coordination of VI) have a radius of 0.605 Å.[35] The radius of Sr cations (in the coordination of XII) is 1.44 Å.[35] Therefore, lattice parameters of the pure $Bi_{1/2}Na_{1/2}TiO_3$ materials should be expanded when

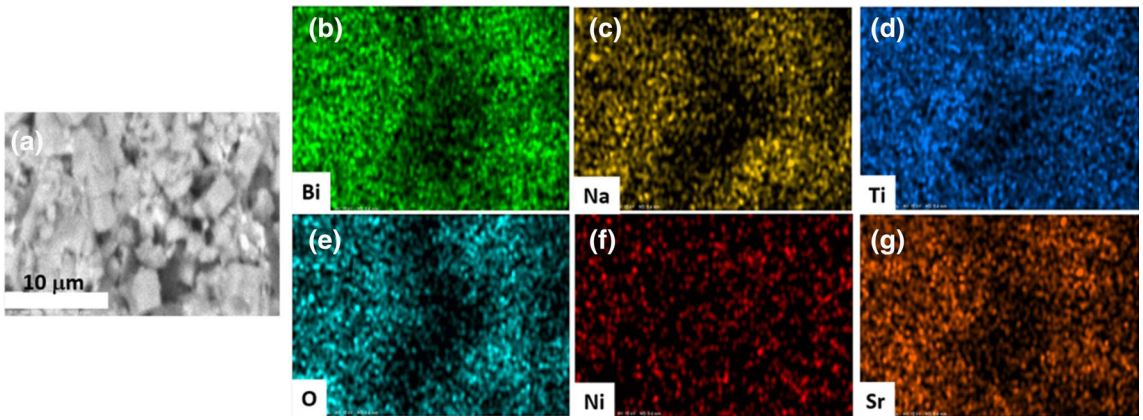

Fig. 2 (a) The selected area for chemical mapping of 5 mol.% $SrNiO_{3-\delta}$-modified $Bi_{1/2}Na_{1/2}TiO_3$ materials, and chemical mappings of (b) Bi, (c) Na, (d) Ti, (e) O, (f) Ni and (g) Sr.

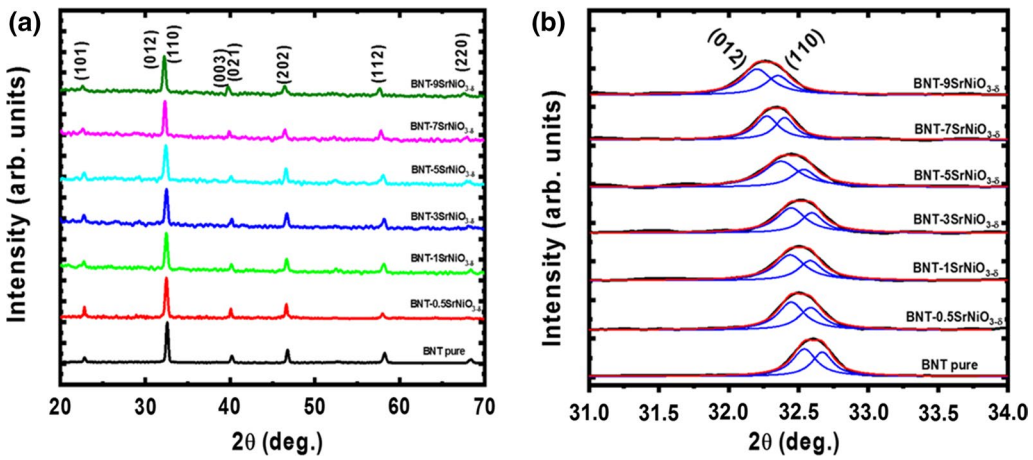

Fig. 3 (a) X-ray diffraction patterns of pure $Bi_{1/2}Na_{1/2}TiO_3$ and $SrNiO_{3-\delta}$-modified $Bi_{1/2}Na_{1/2}TiO_3$ materials with various $SrNiO_{3-\delta}$, concentrations and (b) the magnification with deconvolution of x-ray diffraction patterns in the 2θ-range from 31.0° to 34.0°.

Sr cations were randomly incorporated with Bi- and/or Na-sites. However, unlike Sr cations, Ni cations have complex valance states, and the radius of Ni cations depends on their valence spin states.[35] The radius of Ni^{2+} cations (in the coordination of VI) is 0.690 Å, while radius of Ni^{3+} cations (in the coordination of VI) at the low-spin state and high-spin state are 0.56 Å and 0.60 Å, respectively.[35] In addition, the Ni^{4+} cations (in the same coordination of VI) only existed at a low-spin state with a radius of 0.48 Å.[35] Therefore, the substitution of Ni^{3+} or Ni^{4+} cations for Ti^{4+} resulted in compression of lattice parameters while the substitution of Ni^{2+} cations for Ti^{4+} resulted in expansion lattice parameters. In fact, in addition to the radius difference between the impurity cations and the host cations, numerous other things could affect the lattice parameters as well. Firstly, oxygen vacancies could be created via substituting $Ni^{2+/3+}$ cations for Ti^{4+} and/or by random incorporation of Sr^{2+} cations into Bi^{3+}-sites. The size of oxygen vacancies was estimated at 1.34 Å in the perovskite structure, which is lower than the oxygen anion size of 1.40 Å.[36] Secondly, the random substitution of Sr^{2+} cations for Na^{+} sites resulted in generating Na-vacancies. Both O- and Na-vacancies were suggested to affect the lattice parameters. Thirdly, the Ti^{4+} cations could reduce their valence state to Ti^{3+} and/or even Ti^{2+} by surrounding oxygen vacancies.[37] The reduction in the Ti valence state from 4+ to 3+ or even 2+ should give a certain tension to the lattice because the radius of Ti^{3+} (0.670 Å, in the coordination of VI), and Ti^{2+} (0.86 Å, in the coordination of VI) is larger than that of Ti^{4+} (0.0605 Å, in the coordination of VI).[35] At this time, we cannot identify the main source of the lattice parameter distortion in the $Bi_{1/2}Na_{1/2}TiO_3$ materials via $SrNiO_{3-\delta}$ modification. However, the lattice parameter distortion provided us with solid evidence for the random incorporation of Sr and Ni cations into the $Bi_{1/2}Na_{1/2}TiO_3$ host lattices during solid solution formation.

Figure 4a shows Raman scattering spectra of the pure $Bi_{1/2}Na_{1/2}TiO_3$ and $SrNiO_{3-\delta}$-modified $Bi_{1/2}Na_{1/2}TiO_3$ materials. The Raman scattering peaks overlapped together and appeared as broad bands, which come from the random distribution of Bi and Na cations at *A*-sites in perovskite structure.[38] We tried to distinguish the Raman peaks by using the Lorentzian fitting with *r*-squared greater than 0.99. The deconvolution of Raman scattering peaks is shown in Fig. 4b for the pure BNT, and BNT-$x$$SrNiO_{3-\delta}$ samples with x=1 mol.%, 3 mol.%, and 7 mol.%. The observation of Raman peaks after the deconvolution was well matched with recent results from both theoretical and experimental studies.[18–28,38] Niranjan et al. predicted that low-frequency modes in the range of 109–134 cm^{-1} originated from the displacement of Bi-O ions, modes at higher frequency in the range of 155–187 cm^{-1} were related to Na-O vibrations, whereas vibration modes in the frequency range of 246–401 cm^{-1} were ascribed to TiO_6 vibrations, and modes in the 413–826 cm^{-1} range were ascribed to the vibration of oxygen atoms.[38] Zhu et al. reported that the possible Ti-O vibration modes were in the frequency range of 150–450 cm^{-1} while the TiO_6 vibration modes were assigned to the frequency range of 450–700 cm^{-1}.[39] Domenico et al. and Sczancoski et al. noted that a specific vibration mode at approximately 540 cm^{-1} was reported for O-Ti-O symmetric stretching vibrations of octahedral [TiO_6] clusters, while the distortion mode of [TiO_6] clusters was obtained at around 813 cm^{-1}.[40,41] Barick et al. reported that vibrations of oxygen displacements in perovskite titanate-based materials were dominated by modes at 486 cm^{-1}, 526 cm^{-1}, and 583 cm^{-1}.[42] The shift of vibration modes at approximately 322 cm^{-1} further suggested a distortion of Ti-O or

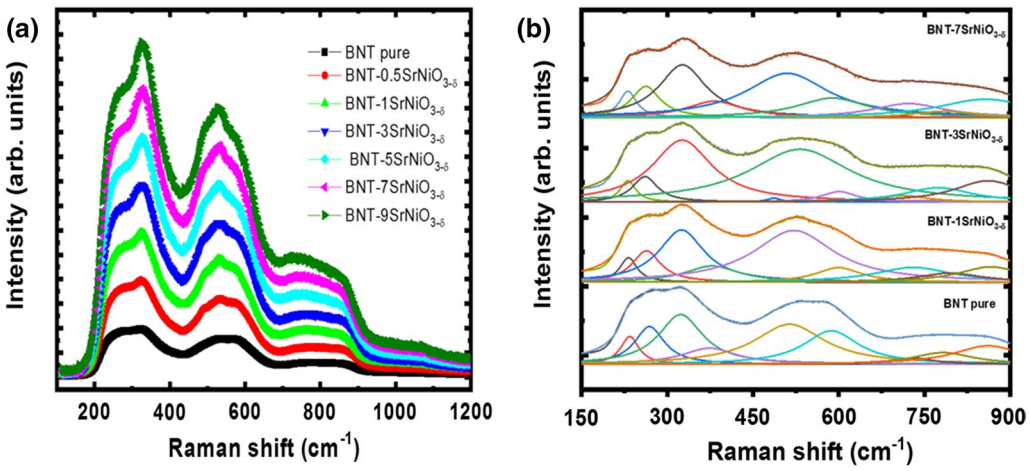

Fig. 4 (a) Raman scattering spectra of pure $Bi_{1/2}Na_{1/2}TiO_3$ and $SrNiO_{3-\delta}$-modified $Bi_{1/2}Na_{1/2}TiO_3$ materials with various $SrNiO_{3-\delta}$ concentrations and (b) deconvolution of Raman scattering peaks for selected $SrNiO_{3-\delta}$-modified $Bi_{1/2}Na_{1/2}TiO_3$ samples.

TiO_6 vibration modes, because Ni cations (molecular mass ~58.69 g/mol) are heavier than Ti cations (~47.87 g/mol). This result is further evidence for substitution of Ni cations in Ti-sites of the host $Bi_{1/2}Na_{1/2}TiO_3$ compounds. The crystal structure studies using X-ray diffraction and Raman scattering confirmed that the $SrNiO_{3-\delta}$ was well incorporated into the host $Bi_{1/2}Na_{1/2}TiO_3$ compounds.

Figure 5a shows the absorption spectra of the pure $Bi_{1/2}Na_{1/2}TiO_3$ and $SrNiO_{3-\delta}$-modified $Bi_{1/2}Na_{1/2}TiO_3$ materials as a function of $SrNiO_{3-\delta}$ concentrations. The spectrum of the pure BNT sample exhibited a single absorption edge with a slight tail. This tail is related to the intrinsic defects from Bi, Na, Ti, or O vacancies and possibly Ti^{3+} .[21] The addition of $SrNiO_{3-\delta}$ into host $Bi_{1/2}Na_{1/2}TiO_3$ materials as solid solutions resulted in a shift of the absorption edge to a higher wavelength, and the appearance of a hump in the range of 600–900 nm. The humps in the absorption spectra of the $SrNiO_{3-\delta}$-modified $Bi_{1/2}Na_{1/2}TiO_3$ materials were related to the presence of Ni cations in the host lattices, which caused electrons to transfer among *3d-3d* orbitals of Ni cations.[16,18,43] Our results are consistent with recent studies on the optical properties of Ni-doped lead-free ferroelectric $Bi_{1/2}K_{1/2}TiO_3$ or $Bi_{1/2}Na_{1/2}TiO_3$ materials.[16,18,43,44] The optical band gap (E_g) was estimated from the absorption spectral data using the Wood-Tauc method.[45] Recently, our theoretical prediction of the electronic structure of $Bi_{1/2}Na_{1/2}TiO_3$ materials indicated that $Bi_{1/2}Na_{1/2}TiO_3$ materials have a direct band gap.[46] Therefore, we used n=1/2 for the Wood-Tauc equation. Thus, the $(\alpha h\nu)^2$ versus photon energy ($h\nu$) is plotted as a function of $SrNiO_{3-\delta}$ content in the solid solutions in Fig. 5b. The estimated E_g values are plotted as a function of $SrNiO_{3-\delta}$ concentrations in the solid solutions in the inset of Fig. 5b. The pure $Bi_{1/2}Na_{1/2}TiO_3$ materials exhibited an approximate E_g value of 3.04 eV, which was consistent with recent observations of $Bi_{1/2}Na_{1/2}TiO_3$ optical band gap in the range of 3.02–3.06 eV.[14–28,43] The addition of $SrNiO_{3-\delta}$ resulted in a reduction of the optical band gap E_g, from 3.04 eV for the pure $Bi_{1/2}Na_{1/2}TiO_3$ sample to 2.63 eV for the 9 mol.% $SrNiO_{3-\delta}$ solid solution. Moreover, E_g values of $Bi_{1/2}Na_{1/2}TiO_3$ materials decreased as a non-monotonic function of $SrNiO_{3-\delta}$ concentration. The reduction of optical band gap might result from complex parameters that could create new states for indirect electron transfer rather than band-to-band electron transitions of the $SrNiO_{3-\delta}$ modified $Bi_{1/2}Na_{1/2}TiO_3$ materials. Both X-ray diffraction and Raman scattering results confirmed that $SrNiO_{3-\delta}$ was well incorporated into the host $Bi_{1/2}Na_{1/2}TiO_3$ crystals, which led to random incorporation of Sr and Ni cations in the host $Bi_{1/2}Na_{1/2}TiO_3$ lattices. Recently, Ref. 16 reported that the incorporation of Ni cations in Ti-sites induced a new local state in the electronic band structure of $Bi_{1/2}Na_{1/2}TiO_3$ materials. In addition, the imbalance of valence states between $Ni^{2+/3+}$ cations and Ti^{4+} cations created oxygen vacancies. Oxygen vacancies reduce the optical band gap because their energy level is located below the conduction band edge in the upper half of the band gap.[21,46] Moreover, *A*-site modification via Sr cations at Bi- and Na-sites during the formation of $SrNiO_{3-\delta}$-$Bi_{1/2}Na_{1/2}TiO_3$ solid solutions affect the electronic band structure of the host $Bi_{1/2}Na_{1/2}TiO_3$ materials in a complicated manner. Firstly, Sr cations at *A*-sites induced a new local state in the electronic band structure of the host $Bi_{1/2}Na_{1/2}TiO_3$ materials. Secondly, the imbalance of valence states between Sr^{2+} and Bi^{3+} cations created oxygen vacancies when Sr^{2+} cations substituted for Bi^{3+} cations, whereas the replacement of Sr^{2+} for Na^+ cations generated Na vacancies. The Na vacancies also induced a new local state in the electronic band structure of $Bi_{1/2}Na_{1/2}TiO_3$ materials.[21] In addition, oxygen vacancies promoted a change of the Ti^{4+}

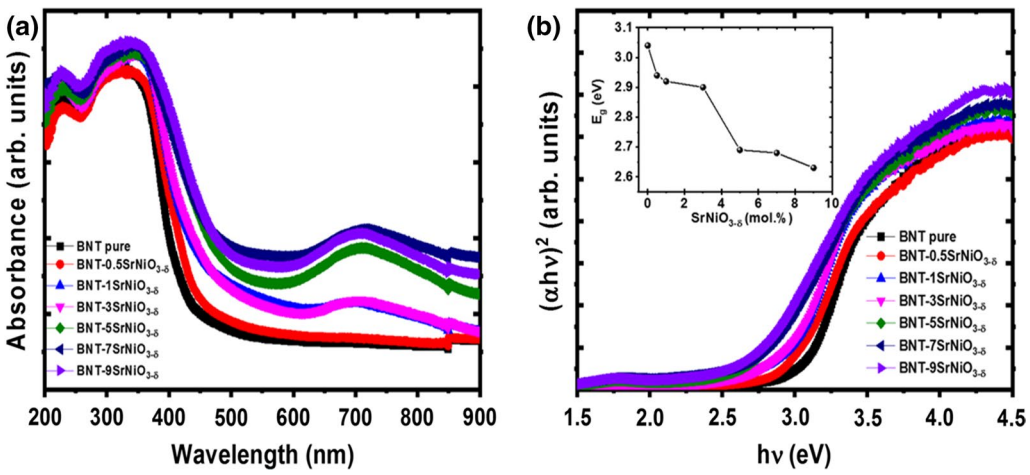

Fig. 5 (a) The absorption spectra and (b) the $(\alpha h\nu)^2$ versus photon energy ($h\nu$) of pure $Bi_{1/2}Na_{1/2}TiO_3$ and $SrNiO_{3-\delta}$-modified $Bi_{1/2}Na_{1/2}TiO_3$ materials with various $SrNiO_{3-\delta}$ concentrations.

valence state to Ti^{3+} (also Ti^{2+}) when they were located around Ti^{4+}.[37] Recently, our theoretical study also predicted that both Ti^{3+} and Ti^{2+} cations can also modify the electronic band structure of $Bi_{1/2}Na_{1/2}TiO_3$ materials.[21] Moreover, the possible valence states of transition metals (e.g. Co, Mn) were recently reported possibly to be changed via compensation with Ti^{3+}-defects, such as $Co^{3+}+Ti^{3+}\rightarrow Co^{2+}+Ti^{4+}$.[47] Therefore, we suggested that the valence states of Ni cations were possibly changed via compensation with Ti^{3+} defects by following the equation $Ni^{3+}+Ti^{3+}\rightarrow Ni^{2+}+Ti^{4+}$. The complex changes in the Ni valence states importantly contributed to the band gap of host $Bi_{1/2}Na_{1/2}TiO_3$ materials. Until now, we could not show the main reason for optical band gap reduction in $Bi_{1/2}Na_{1/2}TiO_3$ materials via a solid solution of $SrNiO_{3-\delta}$. However, the observation of the influence of $SrNiO_{3-\delta}$ concentration on the optical band gap of the host $Bi_{1/2}Na_{1/2}TiO_3$ materials showed solid evidence for random incorporation of Sr and Ni cations into the host lattice during the formation of solid solutions.

The influence of $SrNiO_{3-\delta}$ on the photoemission properties of $Bi_{1/2}Na_{1/2}TiO_3$ materials was also characterized. Figure 6a shows the photoluminescence (PL) spectra of pure $Bi_{1/2}Na_{1/2}TiO_3$ and $SrNiO_{3-\delta}$-modified $Bi_{1/2}Na_{1/2}TiO_3$ materials with various $SrNiO_{3-\delta}$ concentrations. All PL spectra of pure $Bi_{1/2}Na_{1/2}TiO_3$ and $SrNiO_{3-\delta}$-modified $Bi_{1/2}Na_{1/2}TiO_3$ materials exhibited a broadband, where the large photoluminescence intensity was achieved around 480–495 nm. The highest PL peaks were obtained at around 485 nm, as shown in the inset of Fig. 6a where the PL spectra are magnified in the photon wavelength range of 478–505 nm. The addition of $SrNiO_{3-\delta}$ into $Bi_{1/2}Na_{1/2}TiO_3$ materials resulted in PL intensity suppression with increasing the $SrNiO_{3-\delta}$ content, as shown in the inset of Fig. 6a. The dependence of the main PL peaks on $SrNiO_{3-\delta}$ concentration is shown in Fig. 6b, where PL intensity was normalized to the strongest peak. The figure indicates a shift of main peak position with satellite peaks to a higher wavelength with increasing $SrNiO_{3-\delta}$ content. The approximate position of the main peaks at about 485 nm corresponded to the photon energy of 2.56 eV, which is smaller than the band gap of the materials (~3.04 eV). Therefore, we suggested that the main PL peaks did not come from electron transition from the conduction band to the valence band (band-to-band transition). The $Bi_{1/2}Na_{1/2}TiO_3$ materials are ferroelectric that exhibit spontaneous polarization.[1,3] Therefore, hole-electron pair generation from the absorbance of the photon energy was suggested to recombine which prevents photon generation. However, the surface of $Bi_{1/2}Na_{1/2}TiO_3$ materials has un-paired bonding that possibly absorbed electrons, resulting in absorption of the photon energy during recombination with trapped surface defects.[48] The PL intensity of $Bi_{1/2}Na_{1/2}TiO_3$ materials was suppressed by increasing $SrNiO_{3-\delta}$ concentration in the solid solution which was suggested to be related to photon trapping of impurities and/or stress to surface defects.

Furthermore, the role of randomly incorporated Sr and Ni cations on the magnetic properties of the host $Bi_{1/2}Na_{1/2}TiO_3$ materials is shown in Fig. 7. The M-H hysteresis loop of the pure $Bi_{1/2}Na_{1/2}TiO_3$ had an anti-*S*-shape, as shown in Fig. 7a, revealing compensation between diamagnetism and weak ferromagnetism. The diamagnetism of pure $Bi_{1/2}Na_{1/2}TiO_3$ materials originated from an empty state of Ti^{4+} cations, while the weak ferromagnetism was related to self-defects such as Na^+, Bi^{3+} or Ti^{4+} vacancies.[5,14–28] This result was consistent with recent reports on magnetic properties of pure $Bi_{1/2}Na_{1/2}TiO_3$ materials, where the weak ferromagnetism was dominated by intrinsic defects.[3,5,14–28] The addition of $SrNiO_{3-\delta}$ into host $Bi_{1/2}Na_{1/2}TiO_3$ materials induced complex magnetic properties, as shown in Fig. 7b-g

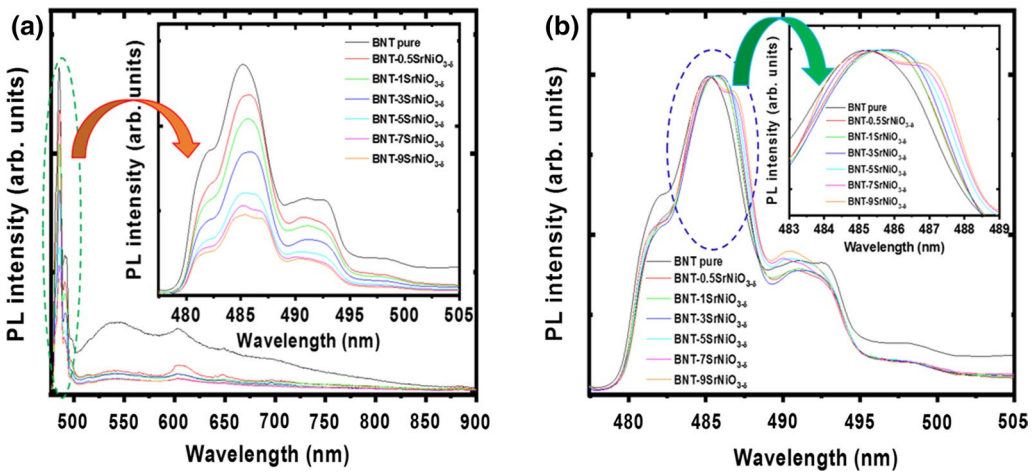

Fig. 6 (a) PL spectra and (b) the normalized PL spectra of pure $Bi_{1/2}Na_{1/2}TiO_3$ and $SrNiO_{3-\delta}$-modified $Bi_{1/2}Na_{1/2}TiO_3$ materials with various $SrNiO_{3-\delta}$ amounts. The insets of (a, b) show the magnification of photoluminescence spectra in the wavelength ranges of 478–505 nm and 483–489 nm, respectively.

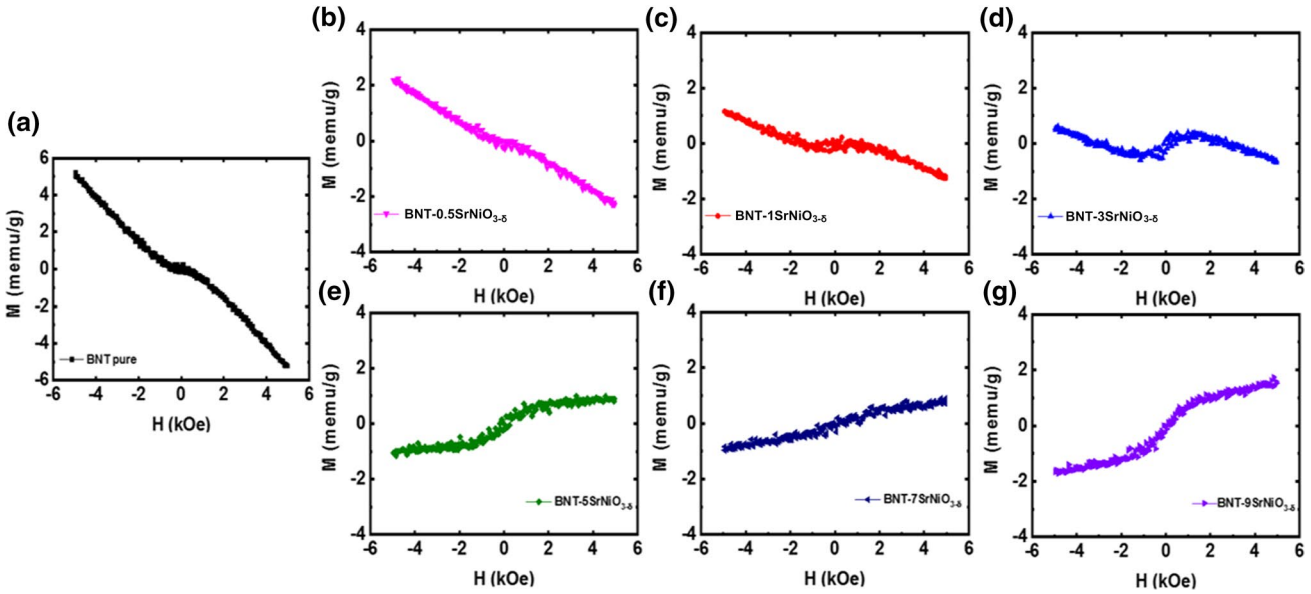

Fig. 7 Magnetic hysteresis loops of (a) pure $Bi_{1/2}Na_{1/2}TiO_3$, and $SrNiO_{3-\delta}$-modified $Bi_{1/2}Na_{1/2}TiO_3$ materials with (b) 0.5 mol.%, (c) 1 mol.%, (d) 3 mol.%, (e) 5 mol.%, (f) 7 mol.% and (g) 9 mol.% $SrNiO_{3-\delta}$ as solid solutions.

for the $SrNiO_{3-\delta}$-modified $Bi_{1/2}Na_{1/2}TiO_3$ materials with 0.5 mol.%, 1 mol.%, 3 mol.%, 5 mol.%, 7 mol.%, and 9 mol.% of $SrNiO_{3-\delta}$, respectively. The diamagnetic signals were suppressed as increasing $SrNiO_{3-\delta}$ concentrations up to 3 mol.%, as shown in Fig. 7b-d. However, the anti-*S*-shape remained in all M-H curves of BNT-xSrNiO$_3$ samples with x=0.5, 1, and 3 mol.%, revealing that the ferromagnetic signal was not high enough in comparison with the diamagnetism signal. Magnetization tended to saturate by increasing the $SrNiO_{3-\delta}$ concentration up to 5 mol.%, as shown in Fig. 7e, which provided solid evidence of typical ferromagnetic behavior. Further addition of $SrNiO_{3-\delta}$ into host $Bi_{1/2}Na_{1/2}TiO_3$ materials showed an unsaturated magnetic moment on the externally applied magnetic field, as shown in Fig. 7f and g for samples with 7 and 9 mol.%, respectively. The observed remnant magnetization (M_r) and coercive field (H_C) values of the pure $Bi_{1/2}Na_{1/2}TiO_3$ and $SrNiO_{3-\delta}$-modified $Bi_{1/2}Na_{1/2}TiO_3$ samples were in the ranges of 0.1–0.2 memu/g and 120–283 Oe, respectively. The non-zero remnant magnetization and coercive field indicated typical ferromagnetism for all studied samples. The complex magnetic behavior of $SrNiO_{3-\delta}$-modified $Bi_{1/2}Na_{1/2}TiO_3$ materials could be explained by assuming random incorporation of Sr and Ni cation impurities into the $Bi_{1/2}Na_{1/2}TiO_3$ host lattices during the formation of solid solutions. The dominant contribution of ferromagnetism in $SrNiO_{3-\delta}$-modified $Bi_{1/2}Na_{1/2}TiO_3$ materials originated from the interactions of Ni cations through oxygen vacancies (□) such as $Ni^{2+/3+}$-□-$Ni^{2+/3+}$ which was reported in transition metal-doped $Bi_{1/2}Na_{1/2}TiO_3$ materials.[14–17] Recently, both experimental and theoretical studies predicted that Ni cations might be stable at a low-spin state when incorporated into $Bi_{1/2}Na_{1/2}TiO_3$ host lattices.[16] Note that the spin magnetic moments of Ni cations at the low spin states of Ni^{2+} ($3d^8 4s^o$), Ni^{3+} ($3d^7 4s^o$), and Ni^{4+} ($3d^6 4s^o$) are 1 μ_B/Ni, 0.5 μ_B/Ni and 0 μ_B/Ni, respectively. Therefore, the highest magnetic moment is obtained for Ni^{2+}-□-Ni^{2+} pair interactions, while the lowest magnetic moment is favored for Ni^{3+}-□-Ni^{3+} pair interactions. However, unlike single-transition-metal-doped $Bi_{1/2}Na_{1/2}TiO_3$ materials, the modification of the *A*-sites (Bi- and Na-sites) by Sr cations also indirectly induced the magnetic moment via complex compensation of valence states between the host and impurity cations. Replacing Sr^{2+} cations for Bi^{3+} cations creates oxygen vacancies, while substituting Sr^{2+} cations for Na^+-sites generates Na vacancies. Recently, both experimental and theoretical studies predicted that Na vacancies induced non-zero magnetic moments.[3,21] Oxygen vacancies indirectly induce the magnetic moments because they facilitate the reduction of the valence state of Ti^{4+} cations to Ti^{3+} or Ti^{2+}.[21,26,37] Ti^{3+} or Ti^{2+} cations had non-zero magnetic moments, which led to the contribution of strong magnetic moments.[14–16,21] Moreover, complex valence transitions were obtained for competition between Ti and Ni cations, including Ni valence reduction from high valence states of $Ni^{3+/4+}$ to a lower valence state of Ni^{2+}, and the valence increase from $Ti^{2+/3+}$ to Ti^{4+} via $Ti^{3+}+Ni^{3+} \rightarrow Ti^{4+}+Ni^{2+}$.[43,47] The change in the valence states of Ni cations was important in changing the number of magnetic moments in $Ni^{2+/3+}$-□-$Ni^{2+/3+}$ pairs. The unsaturated magnetic moment on the applied magnetic field for the BNT-x$SrNiO_{3-\delta}$ samples with high $SrNiO_{3-\delta}$ concentrations could be linked to the contribution

of paramagnetic or antiferromagnetic-like phases. The paramagnetic signal of the high-concentration-$SrNiO_{3-\delta}$-modified $Bi_{1/2}Na_{1/2}TiO_3$ materials originated from Ni isolated cations randomly incorporated into the $Bi_{1/2}Na_{1/2}TiO_3$ host lattices, whereas the antiferromagnetic-like signal might be related to boundary polarons among $Ni^{2+/3+}$-□-$Ni^{2+/3+}$ pairs, such as $Ni^{2+/3+}$-□-$Ni^{2+/3+}$ versus $Ni^{2+/3+}$-□-$Ni^{2+/3+}$. Moreover, we recently obtained strain-mediated ferromagnetic order in antiferromagnetic materials.[49] Therefore, we suggest that the lattice distortion by randomly incorporating Sr and Ni cations into the $Bi_{1/2}Na_{1/2}TiO_3$ host lattices might be affected by the $Ni^{2+/3+}$-□-$Ni^{2+/3+}$ pair interactions or even $Ni^{2+/3+}$-□-$Ni^{2+/3+}$ versus$Ni^{2+/3+}$-□-$Ni^{2+/3+}$ pairs, which resulted in a change of the magnetic ordering magnitude. The origin of ferromagnetic order in $SrNiO_{3-\delta}$-modified $Bi_{1/2}Na_{1/2}TiO_3$ materials is very complex and requires further investigation. However, the observation of room temperature ferromagnetism in lead-free ferroelectric $Bi_{1/2}Na_{1/2}TiO_3$ materials is important for the future application of the materials to smart electronic devices.

For further investigation, ab initio calculation on electronic structures of $SrNiO_{3-\delta}$-modified $Bi_{1/2}Na_{1/2}TiO_3$ materials was performed using CASTEP module in the Materials Studio software.[50] The exchange energy was described by the generalized gradient approximation (GGA) while the potential proposed by Perdew, Burke, and Ernzerhof (PBE)[51] was used for the correlation energy. A 410-eV cutoff energy was used for the plane-wave basis and the *k*-point mesh[52] for the Brillouin sampling is 5×5×2.

Figure 8 shows the unit cells of perfect and Sr/Ni-doped $Bi_{1/2}Na_{1/2}TiO_3$ at different positions. Both *A*-site and *B*-site doping are considered for Sr (see Fig. 8b–d) and Ni (see Fig. 8e-g), and an interstitial doping model was created for the case of Ni doping. Figure 9a illustrates the calculated electronic band structure of pure $Bi_{1/2}Na_{1/2}TiO_3$ with a band gap value of 2.86 eV and the Fermi level just over the top of the valence band. The bottom of the conduction band and the top of valence band occur at the same *k*-point, suggesting that pure $Bi_{1/2}Na_{1/2}TiO_3$ is a direct band gap semiconductor, agreeing with the detailed partial densities of states

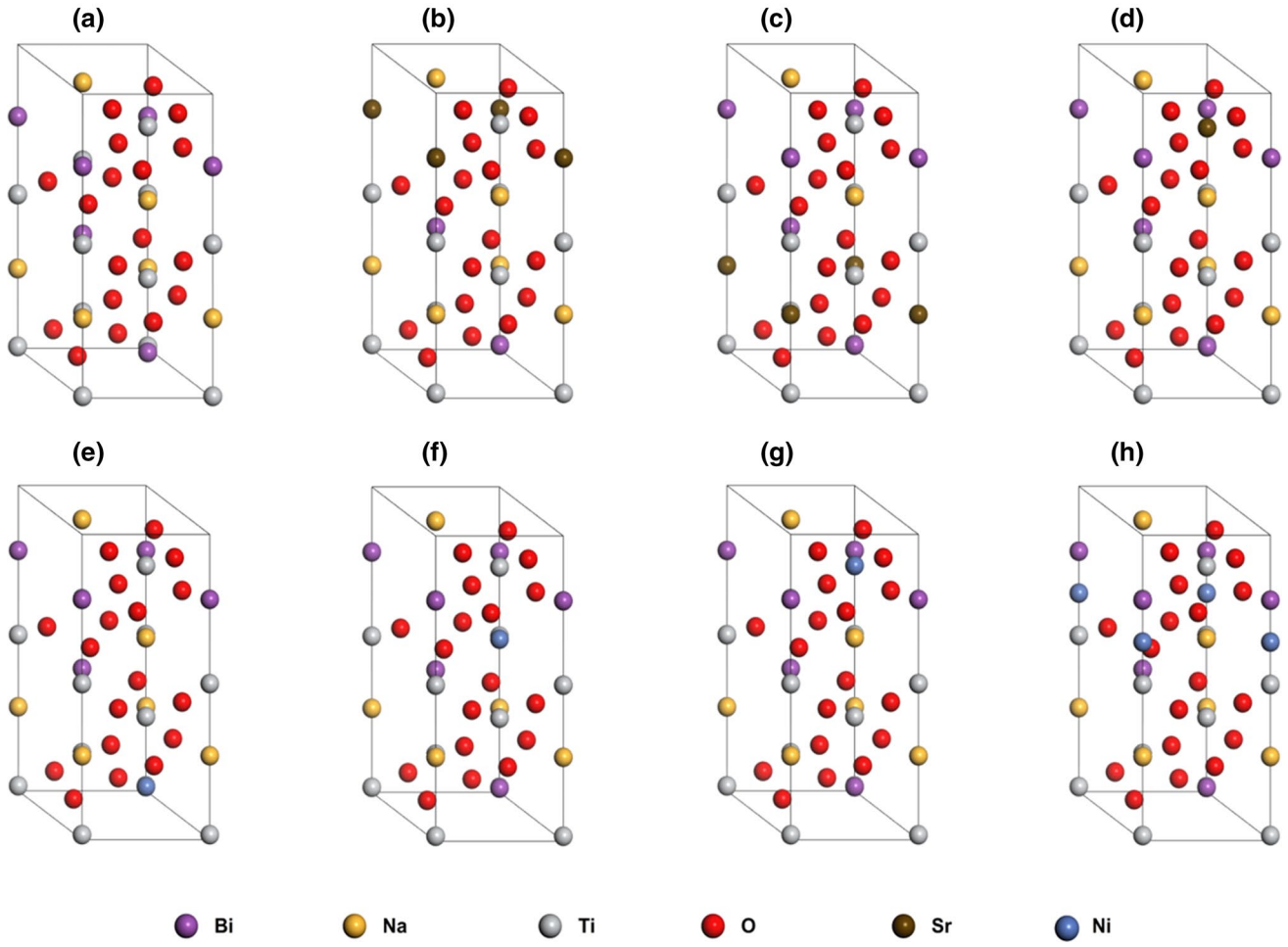

Fig. 8 3D views of the optimized unit cells of (a) pure, (b)-(d) Sr-doped and (e)-(h) Ni-doped $Bi_{1/2}Na_{1/2}TiO_3$ at different sites.

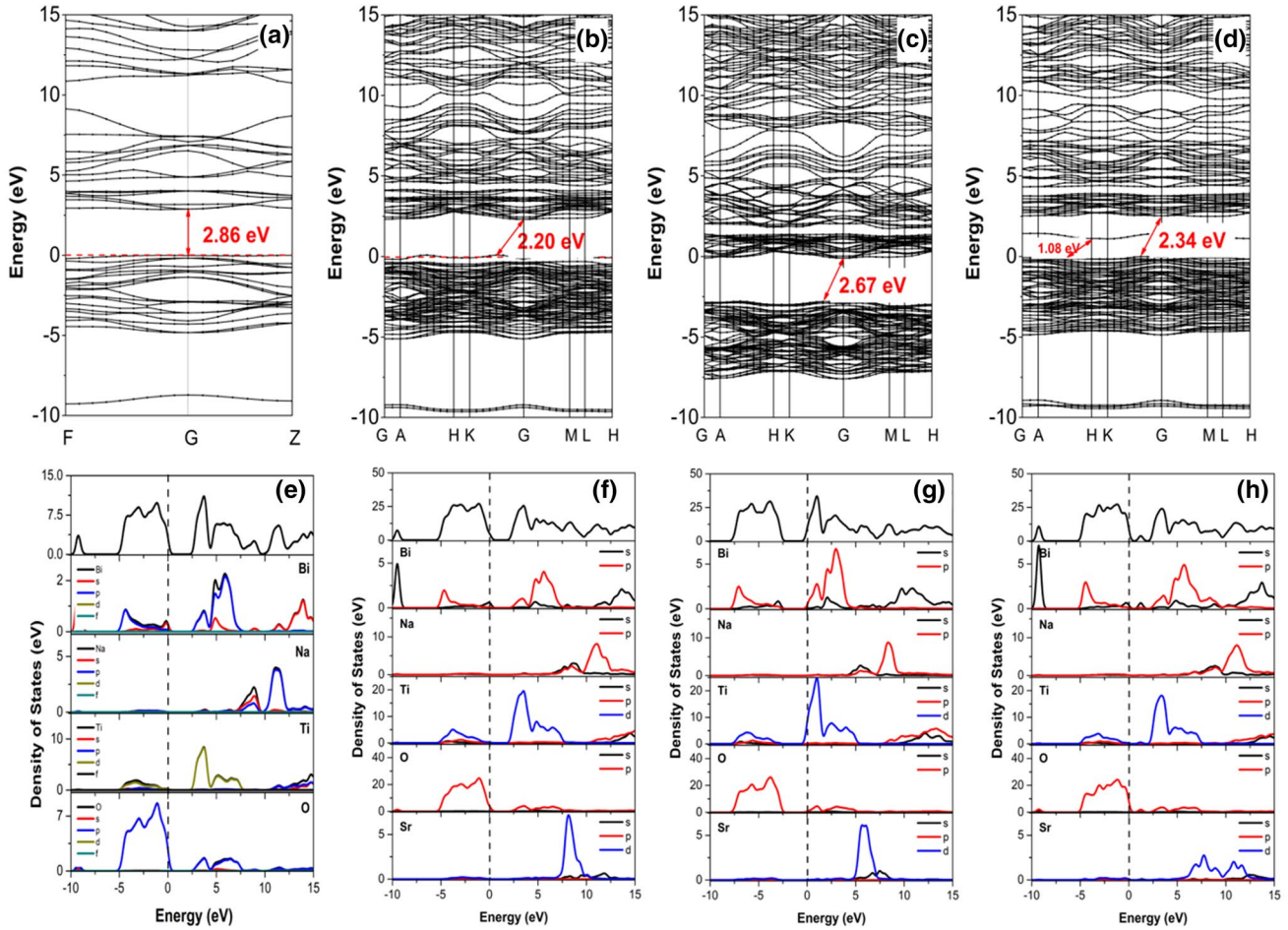

Fig. 9 The DFT results of the spin-resolved total density of states (TDOS) of (a) pure $Bi_{1/2}Na_{1/2}TiO_3$, Sr-doped $Bi_{1/2}Na_{1/2}TiO_3$ at (b) Bi-sites, (c) Na-sites and (d) Ti-sites. The black and red lines represent the spin-up and spin-down orbital states, respectively. The spin density of states of Sr-doped $Bi_{1/2}Na_{1/2}TiO_3$ at (e) Bi-sites and (f) Na-sites. The Fermi level is set to zero energy.

(PDOSs) in Fig. 9a. The band structures of $Bi_{1/2}Na_{1/2}TiO_3$ doped with Sr at Bi-sites, Na-sites and Ti-sites are shown in Fig. 9b-d, respectively. All Sr-doped $Bi_{1/2}Na_{1/2}TiO_3$ materials are indirect band gap semiconductors with a slight shift of the valance highest energy states out of gamma point. The substitution of Sr into host material lattice leads to the reduction of band gap energies; the estimated band gap from the bottom of the conduction bands to the top of valence bands are 2.20 eV, 2.67 eV, and 2.34 eV for Bi-site, Na-site and Ti-site doping positions. The valence bands of Sr-doped $Bi_{1/2}Na_{1/2}TiO_3$ are dominated by the hybridization of O-*2p, Ti-3d,* and Bi-*6p*, but the conduction bands are mainly formed of Bi-6*p*, Ti-3*d,* and O-2*p* orbitals. When doped into host material lattice, Sr atoms contribute to the top of conduction bands via the interaction of Sr-5*s* and Sr-*3d* orbitals. It can be seen that the influence of Sr atoms on Bi-6*s* is the origin of new midgap states in the interstitial doping case of Sr into $Bi_{1/2}Na_{1/2}TiO_3$ lattice, as shown in Fig. 9d, due to the presence of oxygen vacancies.[21,26,53]

Figure 10a-d illustrate the spin-resolved density of states of pure and Sr-doped $Bi_{1/2}Na_{1/2}TiO_3$ at Bi-, Na- and Ti-sites, respectively. All spin-up and spin-down states are degenerate, suggesting that pure and Sr-doped $Bi_{1/2}Na_{1/2}TiO_3$ behave as nonmagnetic materials. Further calculations on the spin density of states of Sr-modified $Bi_{1/2}Na_{1/2}TiO_3$ in Fig. 10e and f indicate that the substitution of Sr atoms into Bi-sites and Na-sites produces small magnetic moments, while none of the magnetic behaviors can be observed with the doping of Sr into Ti-sites or interstitial sites in $Bi_{1/2}Na_{1/2}TiO_3$ material.

Figure 11a-d presents the calculated band structures of $Bi_{1/2}Na_{1/2}TiO_3$ doped with Ni atoms (a) at Bi-sites, (b) Na-sites, (c) Ti-sites and (d) interstitial sites. All Ni-doped $Bi_{1/2}Na_{1/2}TiO_3$ are indirect band gap semiconductors with the corresponding band gap values of 2.62 eV, 2.78 eV, 2.61 eV, and 2.67 eV, calculated from the bottom of conduction bands to the top of valence bands, respectively. The Fermi levels shift to the top of valence bands for Bi-site and

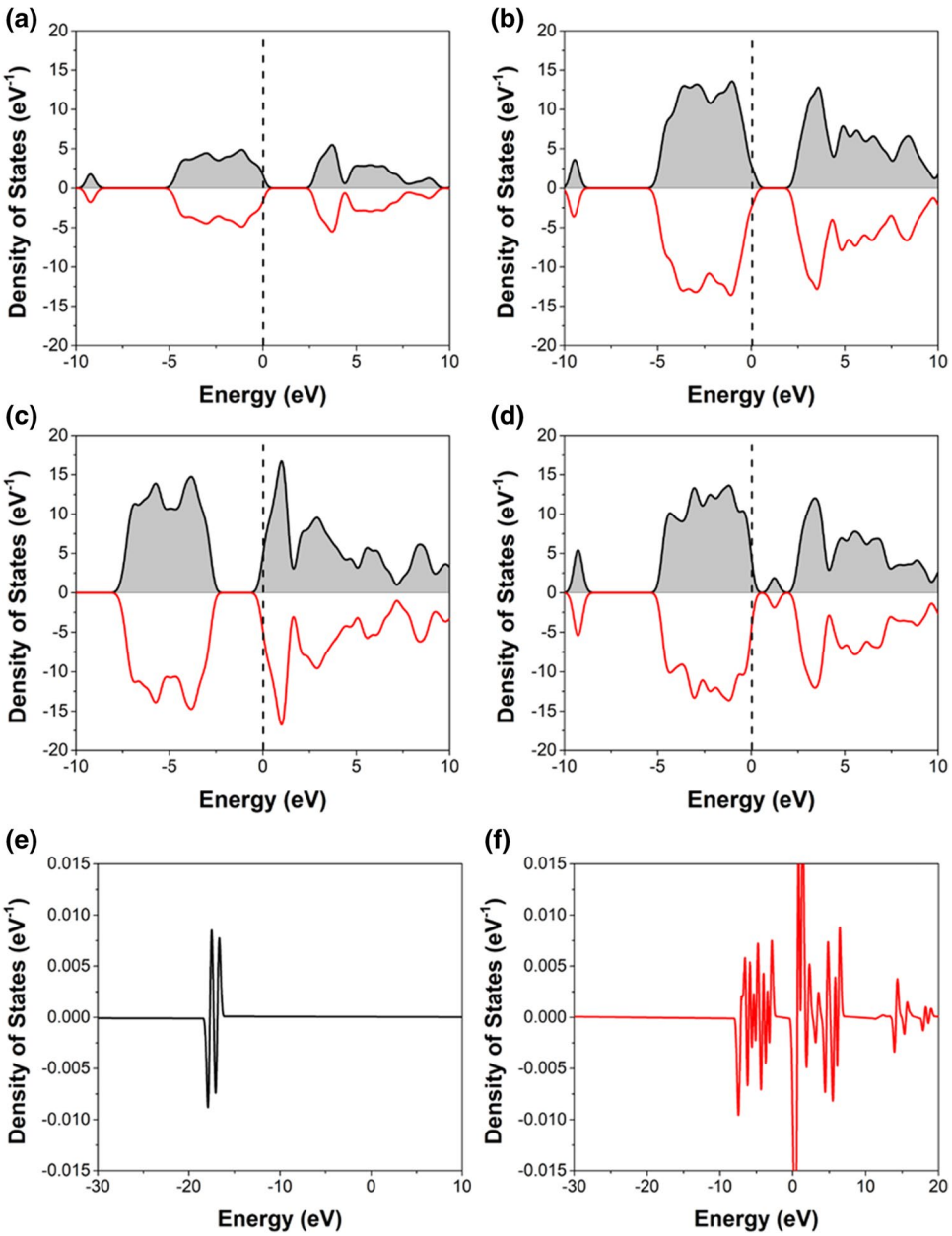

Fig. 10 The DFT results of the spin-resolved total density of states (TDOS) of (a) pure $Bi_{1/2}Na_{1/2}TiO_3$, and Sr-doped $Bi_{1/2}Na_{1/2}TiO_3$ at (b) Bi-sites, (c) Na-sites and (d) Ti-sites; the spin density of states of Sr-doped $Bi_{1/2}Na_{1/2}TiO_3$ at (e) Bi-sites and (f) Na-sites. The black and red lines represent the spin-up and spin-down orbital states, respectively. The Fermi level is set to zero energy.

Ti-site substitutions and lie below the conduction bands for Na-sites and interstitial doping, agreeing with the projected density of states in Fig. 11e-h. It can be seen that the interaction between Ni-*3d* with O-*2p* orbitals leads to the presence of new midgap states, decreasing the optical band gap of doped materials[54–56].

Figure 12 shows the spin-up and spin-down total density of states (TDOSs) of (a) Bi-sites, (b) Na-sites, (c) Ti-sites and (d) interstitial Ni-doped $Bi_{1/2}Na_{1/2}TiO_3$. The symmetric shapes of spin-up and spin-down imply that all states are degenerate and doped $Bi_{1/2}Na_{1/2}TiO_3$ are nonmagnetic materials, except for the case of a Ni atom doped into the site of Na. The clear asymmetry of TDOSs of Na-site doping $Bi_{1/2}Na_{1/2}TiO_3$ indicates a strong magnetic moment for this material. To confirm the magnetic behaviors of Ni-doped $Bi_{1/2}Na_{1/2}TiO_3$ materials, their spin density of states was calculated, the results show that Bi-site and Na-site Ni doping leads to the presence of magnetic properties, opposite to the doping of Ni into Ti-sites or interstitial positions[54–56]. Figure 13a and b presents the contributions of Bi, Na, Ti, O, and Ni atoms to the total spin density of states of Ni-doped $Bi_{1/2}Na_{1/2}TiO_3$ at Bi-sites and Na-sites, suggesting that the magnetic behaviors originated from the Ni dopant, and a small fraction belongs to the neighboring O atoms, consistent with the PDOSs results in Fig. 11a and b. The contour plot of the calculated spin density distribution within a slice passing through the Ni atom in Ni-doped $Bi_{1/2}Na_{1/2}TiO_3$ at Bi-sites and Na-sites are shown in Fig. 13c

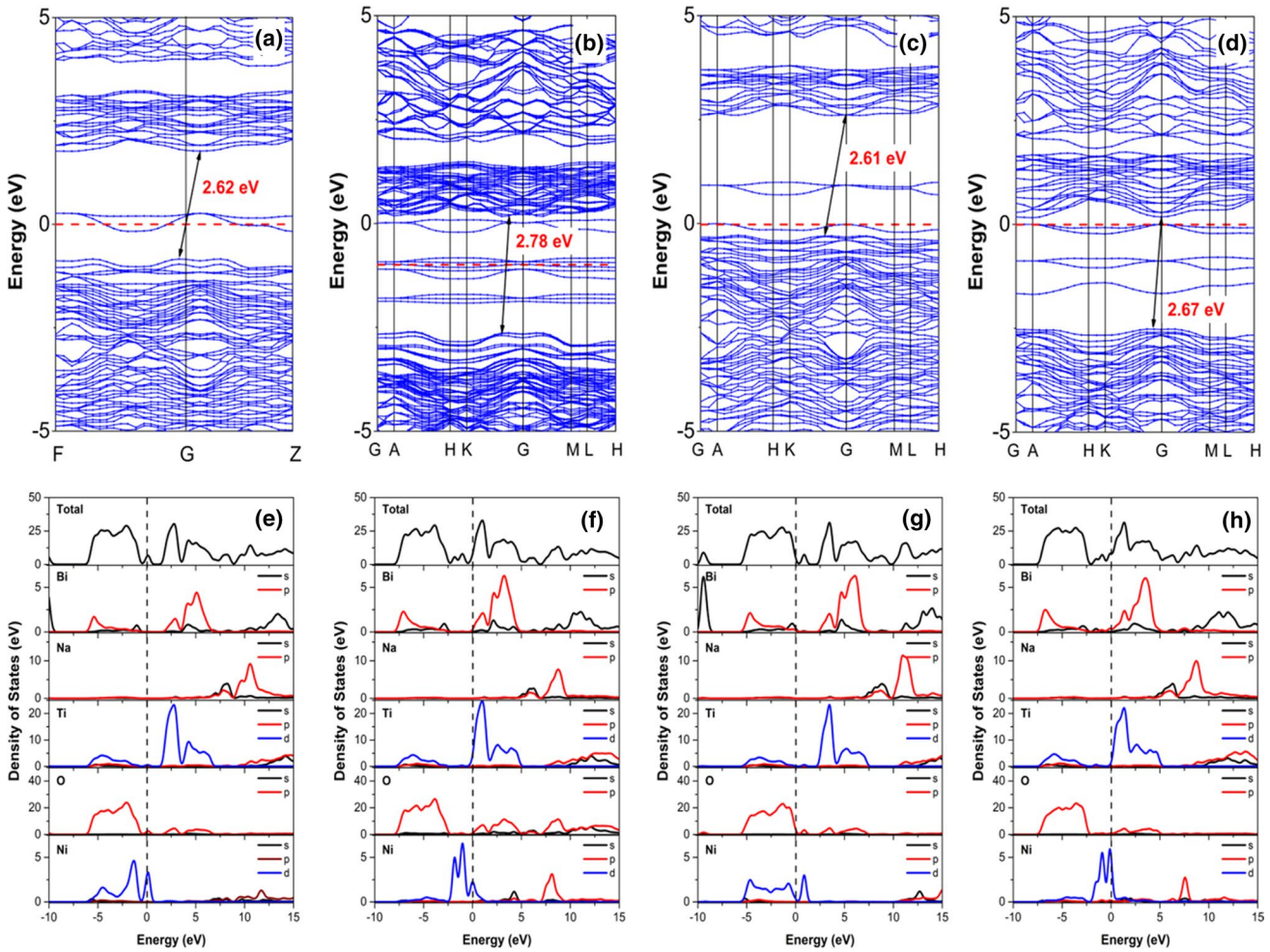

Fig. 11 The DFT results of the band structures of Ni-doped $Bi_{1/2}Na_{1/2}TiO_3$ at (a) Bi-sites, (b) Na-sites, (c) Ti-sites and (d) interstitial. The total density of states and the contribution of Bi, Na, Ti, O, Ni atoms of Ni-doped $Bi_{1/2}Na_{1/2}TiO_3$ at (e) Bi-sites, (f) Na-sites, (g) Ti-sites and (h) interstitial. The Fermi level is set to zero energy.

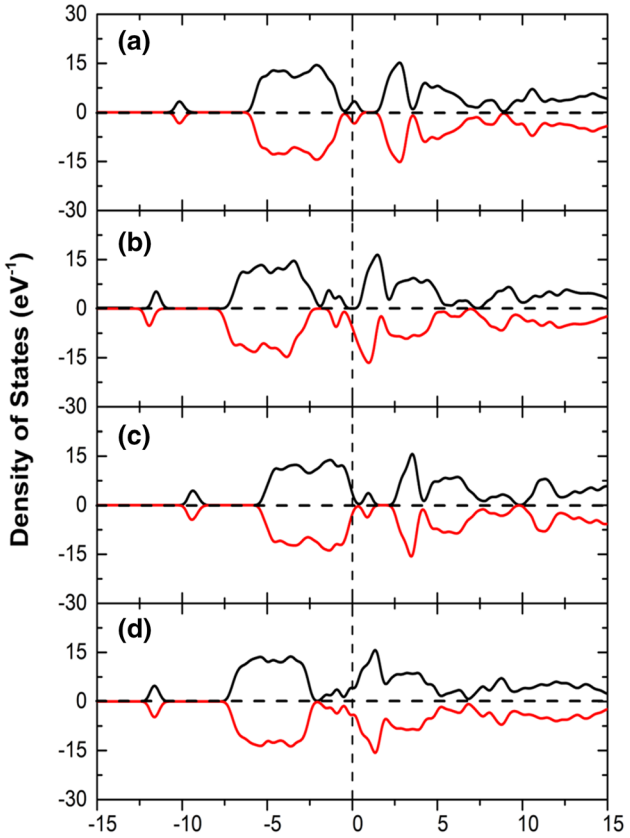

Fig. 12 The DFT results of the spin-resolved total density of states (TDOS) of Ni-doped $Bi_{1/2}Na_{1/2}TiO_3$ at (a) Bi-sites, (b) Na-sites, (c) Ti-sites and (d) interstitial. The black and red lines represent the spin-up and spin-down orbital states, respectively. The Fermi level is set to zero energy.

and d, respectively. It is clear that the increase of spin densities is significant around Ni and O atoms, in good agreement with the spin projected densities of states in Fig. 13a and b. In other words, the substitution of magnetic atoms Ni into the position of Bi or Na in $Bi_{1/2}Na_{1/2}TiO_3$ lattice produces significant magnetic moments in materials.

Conclusion

The $(1-x)Bi_{1/2}Na_{1/2}TiO_3+xSrNiO_{3-\delta}$ solid solutions were synthesized by sol-gel method. The complex magnetic properties were obtained in $SrNiO_{3-\delta}$-modified $Bi_{1/2}Na_{1/2}TiO_3$ materials as a solid solution. The observation of weak ferromagnetism with strongly induced diamagnetism for pure $Bi_{1/2}Na_{1/2}TiO_3$ materials changed to typical ferromagnetism because of the random incorporation of Sr and Ni cations into the host $Bi_{1/2}Na_{1/2}TiO_3$ lattices during the formation of $SrNiO_{3-\delta}$ as solid solutions. The magnetic polaron interaction in the $SrNiO_{3-\delta}$-modified $Bi_{1/2}Na_{1/2}TiO_3$ system was achieved for high $SrNiO_{3-\delta}$ addition. The observation of room-temperature ferromagnetism in the $SrNiO_{3-\delta}$-modified $Bi_{1/2}Na_{1/2}TiO_3$ materials is promising to transfer to smart electronics applications. The DFT calculation predicted that the selection of distribution of Sr and Ni cations into host $Bi_{1/2}Na_{1/2}TiO_3$ crystals at *A*-sites and *B*-sites importantly influenced the electronic structure of host $Bi_{1/2}Na_{1/2}TiO_3$ materials. We expect that our method can be applied for the integration of ferromagnetism in lead-free ferroelectric materials in current developing green multifunctional materials.

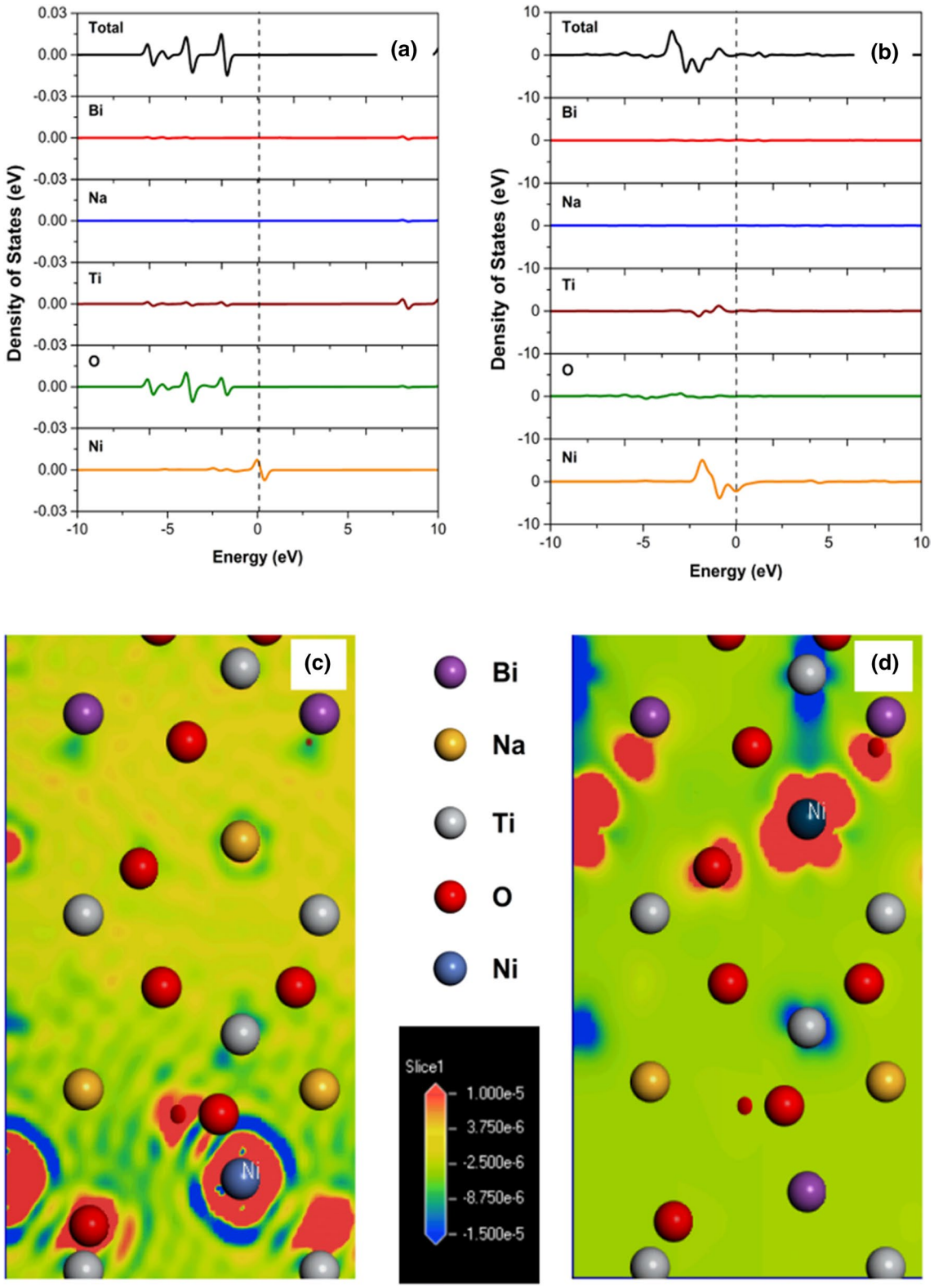

Fig. 13 The DFT results of the spin density of states of Ni-doped $Bi_{1/2}Na_{1/2}TiO_3$ at (a) Bi-sites and (b) Na-sites. Contour plot of the calculated spin density distribution within a slice passing through the Ni atom for Ni-doped $Bi_{1/2}Na_{1/2}TiO_3$ at (c) Bi-sites and (d) Na-sites.

Acknowledgments This research is funded by the Vietnam National Foundation for Science and Technology Development (NAFOSTED) under Grant Number 103.02-2019.366.

Conflict of interest On behalf of all authors, the corresponding author states that there is no conflict of interest.

References

1. N.D. Quan, L.H. Bac, D.V. Thiet, V.N. Hung, and D.D. Dung, Current development in lead-free $Bi_{0.5}(Na,K)_{0.5}TiO_3$-based piezoelectric materials. *Adv. Mater. Sci. Eng.* 2014, 365391 (2014).
2. S. Tong, Y.E. von Schirnding, and T. Prapamontol, Environmental lead exposure: a public health problem of global dimensions. *Bull. World Health Organ.* 78, 1068 (2000).
3. L. Ju, C. Shi, L. Sun, Y. Zhang, H. Qin, and J. Hu, Room-temperature magnetoelectric coupling in nanocrystalline $Na_{0.5}Bi_{0.5}TiO_3$. *J. Appl. Phys.* 116, 083909 (2014).
4. M.M. Vopson, Fundamentals of multiferroic materials and their possible applications. *Crit. Rev. Solid State Mater. Sci.* 40, 223 (2015).
5. L.T.H. Thanh, N.B. Doan, N.Q. Dung, L.V. Cuong, L.H. Bac, N.A. Duc, P.Q. Bao, and D.D. Dung, Origin of room temperature ferromagnetism in Cr-doped lead-free ferroelectric $Bi_{0.5}Na_{0.5}TiO_3$ materials. *J. Electron. Mater.* 46, 3367 (2017).
6. M. Bichurin, V. Petrov, A. Zakharov, D. Kovalenko, S.C. Yang, D. Maurya, V. Bedekar, and S. Priya, Magnetoelectric interactions in lead-based and lead-free composites. *Materials* 4, 651 (2011).
7. P. Jarupoom and P. Jaita, Enhanced magnetic performance of lead-free $(Bi_{0.5}Na_{0.5})TiO_3$-$CoFe_2O_4$ magnetoelectric ceramics. *Electron. Mater. Lett.* 11, 788 (2015).
8. S.N. Babu, J.H. Hsu, Y.S. Chen, and J.G. Lin, Magnetoelectric response in lead-free multiferroic $NiFe_2O_4$–$Na_{0.5}Bi_{0.5}TiO_3$ composites. *J. Appl. Phys.* 109, 07D904 (2011).
9. M. Kumari, A. Singh, A. Gupta, C. Prakash, and R. Chatterjee, Self-biased large magnetoelectric coupling in co-sintered $Bi_{0.5}Na_{0.5}TiO_3$ based piezoelectric and $CoFe_2O_4$ based magnetostrictive bilayered composite. *J. Appl. Phys.* 116, 244101 (2014).
10. M. Tyagi, P. Sharma, M. Kumari, and M. Thakur, Improved magnetoelectric effect in lead free $[72.5(Bi_{1/2}Na_{1/2}TiO_3)$–$22.5(Bi_{1/2}K_{1/2}TiO_3)$–$5(BiMg_{1/2}Ti_{1/2}O_3)]$: $CoFe_2O_4$ particulate nanocomposites prepared by sol–gel method. *J. Mater. Sci. Mater. Electron.* 28, 2812 (2017).
11. L.G. Wang, X.X. Wang, C.M. Zhu, G.B. Yu, Y.T. Zhao, Z.H. Huang, W.J. Kong, F.C. Liu, and F.Z. Lv, Influences of annealing temperature on dielectric, magnetic and magnetoelectric coupling properties of $0.7Bi_{0.5}Na_{0.5}TiO_3$-$0.3NiFe_2O_4$ ceramics. *J. Magn. Magn. Mater.* 494, 165773 (2020).
12. Y. Wang, G. Xu, L. Yang, Z. Ren, X. Wei, W. Weng, P. Du, G. Shen, G. Shen, and G. Han, Room-temperature ferromagnetism in Fe-doped $Na_{0.5}Bi_{0.5}TiO_3$ crystals. *Mater. Sci. Poland* 27, 471 (2009).
13. Y. Wang, G. Xu, X. Ji, Z. Ren, W. Weng, P. Du, G. Shen, and G. Han, Room-temperature ferromagnetism of Co-doped $Na_{0.5}Bi_{0.5}TiO_3$: Diluted magnetic ferroelectrics. *J. Alloys Compd.* 475, L25 (2009).
14. D.D. Dung, N.B. Doan, N.Q. Dung, N.H. Linh, L.H. Bac, L.T.H. Thanh, N.N. Trung, N.V. Duc, L.V. Cuong, D.V. Thiet, and S. Cho, Tunable magnetism of $Na_{0.5}Bi_{0.5}TiO_3$ materials via Fe defects. *J. Supercond. Novel Magn.* 32, 3011 (2019).
15. D.D. Dung, N.B. Doan, N.Q. Dung, L.H. Bac, L.T.H. Thanh, D.V. Thiet, N.N. Trung, N.C. Khang, T.V. Trung, and N.V. Duc, Role of Co dopants on the structural, optical and magnetic properties of lead-free ferroelectric $Na_{0.5}Bi_{0.5}TiO_3$ materials. *J. Sci. Adv. Mater. Dev.* 4, 584 (2019).
16. D.D. Dung, N.Q. Dung, N.B. Doan, N.H. Linh, L.H. Bac, N.N. Trung, N.V. Duc, L.T.H. Thanh, L.V. Cuong, D.V. Thiet, and S. Cho, Defect-mediated room temperature ferromagnetism in lead-free ferroelectric $Na_{0.5}Bi_{0.5}TiO_3$ materials. *J. Supercond. Novel Magn.* 33, 911 (2020).
17. L.T.H. Thanh, N.B. Doan, L.H. Bac, D.V. Thiet, S. Cho, P.Q. Bao, and D.D. Dung, Making room-temperature ferromagnetism in lead-free ferroelectric $Bi_{0.5}Na_{0.5}TiO_3$ material. *Mater. Lett.* 186, 239 (2017).
18. M.M. Hue, N.Q. Dung, N.N. Trung, L.H. Bac, L.T.K. Phuong, N.V. Duc, and D.D. Dung, Tunable magnetic properties of $Bi_{0.5}Na_{0.5}TiO_3$ materials via solid solution of $NiTiO_3$. *Appl. Phys. A* 124, 588 (2018).
19. M.M. Hue, N.Q. Dung, L.T.K. Phuong, N.N. Trung, N.V. Duc, L.H. Bac, and D.D. Dung, Magnetic properties of $(1–x)Bi_{0.5}Na_{0.5}TiO_3$+$x$$MnTiO_3$ materials. *J. Magn. Magn. Mater.* 471, 164 (2019).
20. D.D. Dung, M.M. Hue, N.Q. Dung, N.H. Lam, L.T.K. Phuong, L.H. Bac, N.N. Trung, N.V. Duc, and D. Odkhuu, Enhancing room-temperature ferromagnetism in $Bi_{0.5}Na_{0.5}TiO_3$ via $FeTiO_3$ solid solution. *J. Electroceram.* 44, 129 (2020).
21. N.T. Hung, N.H. Lam, A.D. Nguyen, L.H. Bac, N.N. Trung, D.D. Dung, Y.S. Kim, N. Tsogbadrakh, T. Ochirkhuyag, and D. Odkhuu, Intrinsic and tunable ferromagnetism in $Bi_{0.5}Na_{0.5}TiO_3$ through $CaFeO_{3-\delta}$ modification. *Sci. Rep.* 10, 6189 (2020).
22. N.T. Hung, L.H. Bac, N.N. Trung, N.T. Hoang, P.V. Vinh, and D.D. Dung, Room-temperature ferromagnetism in Fe-based perovskite solid solution in lead-free ferroelectric $Bi_{0.5}Na_{0.5}TiO_3$ materials. *J. Magn. Magn. Mater.* 451, 183 (2018).
23. N.T. Hung, L.H. Bac, N.T. Hoang, P.V. Vinh, N.N. Trung, and D.D. Dung, Structural, optical, and magnetic properties of $SrFeO_{3-\delta}$-modified $Bi_{0.5}Na_{0.5}TiO_3$ materials. *Physica B: Conden. Matt.* 531, 75 (2018).
24. D.D. Dung, N.T. Hung, and D. Odkhuu, Magnetic and optical properties of $MgMnO_{3-\delta}$-modified $Bi_{0.5}Na_{0.5}TiO_3$ materials. *J. Magn. Magn. Mater.* 482, 31 (2019).
25. D.D. Duc, N.T. Hung, and D. Odkhuu, Magnetic and optical properties of new $(1–x)$ $Bi_{0.5}Na_{0.5}TiO_3$ + $x$$BaMnO_{3-\delta}$ solid solution materials. *Appl. Phys. A* 125, 465 (2019).
26. D.D. Dung, N.T. Hung and D. Odkhuu, Structure, optical and magnetic properties of new $Bi_{0.5}Na_{0.5}TiO_3$-$SrMnO_{3-\delta}$ solid solution materials. *Sci. Rep.* 9, 18186 (2019).
27. D.D. Dung and N.T. Hung, Structural, optical, and magnetic properties of the new $(1–x)Bi_{0.5}Na_{0.5}TiO_3$+$xMgCoO_{3-\delta}$ solid solution system. *J. Supercond. Novel Magn.* 33, 1249 (2020).
28. D.D. Dung and N.T. Hung, Magnetic properties of $(1–x)$ $Bi_{0.5}Na_{0.5}TiO_3$ + $x$$SrCoO_{3-\delta}$ solid-solution materials. *Appl. Phys. A* 126, 240 (2020).
29. A.A. Demkov, and A.B. Posadas, *Integration of Functional Oxides with Semiconductors*, 2014th ed., (New York: Springer, 2014).
30. M. Rahman, K.C. Zhou, Y.Z. Nie, and G.H. Guo, Electronic structure and magnetism of layered compounds $SrBO_2$ (B= Ni Co, Mn): a theoretical investigation. *Solid State Commun.* 266, 6 (2017).
31. M. Zinkevich, Constitution of the Sr–Ni–O system. *J. Solid State Chem.* 178, 2818 (2005).
32. Y. Takeda, T. Hashino, H. Miyamoto, F. Kanamaru, S. Kume, and M. Koizumi, Synthesis of $SrNiO_3$ and related compound, $Sr_2Ni_2O_5$. *J. Inorg. Nuclear Chem.* 34, 1599 (1972).
33. G.Y. Chen, C.L. Ma, D. Chen, and Y. Zhu, Robust half-metallicity of hexagonal $SrNiO_3$. *J. Solid State Chem.* 233, 438 (2016).
34. V.I. Anisimov, D. Bukhvalov, and T.M. Rice, Electronic structure of possible nickelate analogs to the cuprates. *Phys. Rev. B* 59, 7901 (1999).

35. R.D. Shannon, Revised effective ionic radii and systematic studies of interatomic distances in halides and chalcogenides. *Acta Cryst. A* 32, 751 (1976).
36. C. Chatzichristodoulou, P. Norby, P.V. Hendriksen, and M.B. Mogensen, Size of oxide vacancies in fluorite and perovskite structured oxides. *J. Electroceram.* 34, 100 (2015).
37. X. Liu, H. Fan, J. Shi, L. Wang, and H. Du, Enhanced ionic conductivity of Ag addition in acceptor-doped $Bi_{0.5}Na_{0.5}TiO_3$ ferroelectrics. *RSC Adv.* 6, 30623 (2016).
38. M.K. Niranjan, T. Karthik, S. Asthana, J. Pan, and U.V. Waghmare, Theoretical and experimental investigation of Raman modes, ferroelectric and dielectric properties of relaxor $Na_{1/2}Bi_{1/2}TiO_3$. *J. Appl. Phys.* 113, 194106 (2013).
39. J. Zhu, J. Zhang, K. Jiang, H. Zhang, Z. Hu, H. Luo, and J. Chu, Coexistence of ferroelectric phases and phonon dynamics in relaxor ferroelectric $Na_{0.5}Bi_{0.5}TiO_3$ based single crystals. *J. Am. Ceram. Soc.* 99, 2408 (2016).
40. M.D. Domenico Jr., S.H. Wemple, S.P.S. Porto, and P.R. Buman, Raman spectrum of single-domain $BaTiO_3$. *Phys. Rev.* 174, 522 (1968).
41. J.C. Sczancoski, L.S. Cavalcante, T. Badapanda, S.K. Rout, S. Panigrahi, V.R. Mastelaro, J.A. Varela, M.S. Li, and E. Longo, Structure and optical properties of $[Ba_{1-x}Y_{2x/3}](Zr_{0.25}Ti_{0.75})O_3$ powders. *Solid State Sci.* 12, 1160 (2010).
42. B.K. Barick, K.K. Mishra, A.K. Arora, R.N.P. Choudhary, and D.K. Pradhan, Impedance and Raman spectroscopic studies of $(Na_{0.5}Bi_{0.5})TiO_3$. *J. Phys. D: Appl. Phys.* 44, 355402 (2011).
43. D.D. Dung, M.M. Hue, N.Q. Dung, L.T.K. Phuong, L.H. Bac, N.X. Duong, P.D. Luong, N.A. Duc, N.N. Trung, N.H. Thoan, and D. Odkhuu, Influenced of $Bi(Ti_{1/2}Ni_{1/2})O_3$ concentration on the structural, optical and magnetic properties of lead-free $Bi_{1/2}Na_{1/2}TiO_3$ materials. *Vacuum* 177, 109306 (2020).
44. D.V. Thiet, D.D. Cuong, L.H. Bac, L.V. Cuong, H.D. Khoa, S. Cho, N.H. Tuan, and D.D. Dung, Room-temperature ferromagnetism in nickel-doped wide dand gap ferroelectric $Bi_{0.5}K_{0.5}TiO_3$ nanocrystals. *Mater. Trans.* 56, 1339 (2015).
45. D.L. Wood and J. Tauc, Weak absorption tails in amorphous semiconductors. *Phys. Rev. B* 5, 3144 (1972).
46. N.H. Linh, N.H. Tuan, D.D. Dung, P.Q. Bao, B.T. Cong and L.T.H. Thanh, Alkali metal-substituted bismuth-based perovskite compounds: A DFT study. *J. Sci. Adv. Mater. Dev.* 4, 492 (2019).
47. V. Schmitt and F. Raether, Effect of cobalt doping on the sintering mechanisms of the lead-free piezoceramic $(Bi_{0.5}Na_{0.5})TiO_3$. *J. European Ceram. Soc.* 34, 15 (2014).
48. Y. Lin, C.W. Nan, J. Wang, H. He, J. Zhai and L. Jiang, Photoluminescence of nanosized $Na_{0.5}Bi_{0.5}TiO_3$ synthesized by a sol–gel process. *Mater. Lett.* 58, 829 (2004).
49. D.D. Dung, D.V. Thiet, D.A. Tuan, and S. Cho, Strain effects in epitaxial Mn_2O_3 thin film grown on MgO(100). *J. Appl. Phys.* 113, 17A314 (2013).
50. S.J. Clark, M.D. Segall, C.J. Pickard, P.J. Hasnip, M.J. Probert, K. Refson, and M.C. Payne, First principles methods using CASTEP. *Z. Kristallogr.* 220, 567 (2005).
51. J.P. Perdew, K. Burke, and M. Ernzerhof, Generalized Gradient Approximation Made Simple. *Phys. Rev. Lett.* 77, 3865 (1996).
52. H.J. Monkhorst and J.D. Pack, Special points for Brillouin-zone integrations. *Phys. Rev. B* 13, 5188 (1976).
53. D.D. Dung, N.H. Lam, A.D. Nguyen, N.N. Trung, N.V. Duc, N.T. Hung, Y.S. Kim, and D. Odkhuu, Experimental and theoretical studies on induced ferromagnetism of new $(1-x)Na_{0.5}Bi_{0.5}TiO_3 + xBaFeO_{3-\delta}$ solid solution. *Sci. Rep.* 11, 8908 (2021).
54. D.D. Dung, N.H. Thoan, N.Q. Dung, P.V. Vinh, N.H. Lam, V.T. Lam, P.D. Luong, and D.Q. Van, Magnetic properties of a (1-x) $Bi_{0.5}Na_{0.5}TiO_3+xCaNiO_{3-\delta}$ solid solution system prepared by sol-gel technique, *J. Electron. Mater.* (2022). https://doi.org/10.1007/s11664-022-09457-2
55. D.D. Dung, N.H. Thoan, N.Q. Dung, N.H. Lam, P.V. Vinh, V.T. Lam, P.D. Luong, and D.Q. Van, Structural, optical, and magnetic properties of a new complex $(1-x)Bi_{1/2}Na_{1/2}TiO_3+xMgNiO_{3-\delta}$ solid solution system, *Appl. Phys. A* 128, 129 (2022).
56. D.D. Dung, N.H. Thoan, P.V. Vinh, N.H. Lam, V.T. Lam, P.D. Luong, D.Q. Van, and D. Odkhuu, Magnetic properties of new $(1-x)Bi_{1/2}Na_{1/2}TiO_3+xBaNiO_{3-\delta}$ solid solution materials, *Appl. Phys. A* 128, 168 (2022)